Thermochimica Acta 730 (2023) 179617

Contents lists available at ScienceDirect

Thermochimica Acta

journal homepage: www.elsevier.com/locate/tca

Thermal and structural properties of polyzwitterions: Effects of monomer chemistry and salt addition

John Thomas [a], Sammie Chum [a], William Deucher [a], Abhishek Mondal [b], Ayse Asatekin [b], Peggy Cebe [a,*]

[a] Department of Physics and Astronomy, Tufts University, Medford, MA, United States
[b] Department of Chemical and Biological Engineering, Tufts University, Medford, MA, United States

ARTICLE INFO

Keywords:
Polyzwitterion
LiCl salt
Crosslinking and confinement
Glass transition temperature
Heat capacity
Bound water

ABSTRACT

Thermal and structural properties of polyzwitterions (PZI)s comprising the sulfobetaine moiety were studied as a function of LiCl addition and variations in monomer chemistry. The polyzwitterions chosen for this study are: poly(sulfobetaine methacrylate), PSBMA; poly(sulfobetaine acrylate), PSBA; and, poly(ethyl sulfobetaine methacrylate), PESBMA. When LiCl salt is added, the $Li^+$and Cl^- ions disrupt the dipole-dipole electrostatic interaction of the PZI side groups. Fourier transform infrared spectroscopy shows that the vibrational frequencies of the symmetric and asymmetric *S=O* bonds increase as LiCl content increases. Structural studies by wide angle X-ray scattering show that all the PZIs are amorphous, and the average interatomic spacing, d, increases in the order: d_{PSBA}(= 0.456±0.006nm) < d_{PSBMA} (= 0.474±0.015nm) < d_{PESBMA} (= 0.493±0.011nm). Upon the addition of LiCl, d-spacing for a given PZI decreases as LiCl content increases. Thermogravimetry showed that PZIs had degradation onset temperatures $T_d \sim 300°C$. As LiCl content increases, the onset temperature of degradation decreases suggesting that the disruption of dipole-dipole crosslinks destabilizes the polymer. All the PZIs are hydrophilic and hygroscopic, and a drying procedure was developed so that well-defined glass-to-liquid transitions could be observed in the dry solid state. PZIs without LiCl have glass transition temperatures, T_g, increasing in the order: $T_{g,PSBA}$(= 200±1°C) < $T_{g,PESBMA}$ (= 204±1°C) < $T_{g,PSBMA}$ (= 237±1°C). As the LiCl content increases, T_g decreases, and the liquid state heat capacity increases, in all PZIs. The specific heat capacity increment at T_g was studied for PSBA as a function of LiCl content. In PSBA, the heat capacity increment reached a maximum for molar ZI:LiCl content at and above 1:1, and its value agreed well with predictions based on an empirical bead model of polymers. Thermal data on the dry state of PZI-LiCl complexes suggest an analogy between electrostatically crosslinked, fully amorphous PZIs and semicrystalline polymers. The dipolar crosslinks confine the molecular motion of PZIs just as crystal domains confine the molecular motion of the amorphous phase in semicrystalline polymers.

1. Introduction

Polyzwitterions (PZIs) are a subcategory of polyampholytes in which the monomeric repeat unit contains an equal number of positively and negatively charged groups that are covalently linked with each other, in either the backbone or the side-groups [1,2]. Most zwitterionic groups are hydrophilic. For instance, the hydrophilic end groups of phospholipids are zwitterions. Hydrophilicity enhances polyzwitterion biocompatibility, which allows them to be used in wound dressings and drug delivery systems [3–7]. PZI hydrophilicity also imparts resistance to biofouling, which is important for their use in filtration membranes [8, 9].

The polyzwitterions in this study contain a zwitterionic moiety in the side group of each repeat unit. Due to the separation of charges on the side group, these groups form strong dipole-dipole electrostatic crosslinks, as shown schematically in Fig. 1a [1,2]. Dipolar crosslinking results in a fully amorphous conformation showing no long-range order. The crosslinks stabilize the polymer chains resulting in high glass transition and degradation temperatures [10,11]. Along with the formation of dipolar crosslinks, these charged side groups allow the PZI to dissolve molar ratios of salt making them candidates for use as solid polymer electrolytes [12–15].

* Corresponding author.
E-mail address: peggy.cebe@tufts.edu (P. Cebe).

https://doi.org/10.1016/j.tca.2023.179617
Received 15 August 2023; Received in revised form 7 October 2023; Accepted 9 October 2023
Available online 10 October 2023

Upon the addition of LiCl salt, the intra- and inter-molecular crosslinking can be disrupted, as shown in Fig. 1b. The free $Li^+$and Cl^- ions associate onto the charged side groups moderating the formation of dipolar crosslinking. Cardoso, et al. [12] have shown that for a variety of salts, including LiCl, as salt content increases, the glass transition temperature increases in poly(sulfobetaine of [*sic*] 12-ethyl-3,6,9-triox-a-12-azatetradec-1-yl 2-methylacrylate) (called PMBS-4 in reference 12). Other studies [16–19] have shown that larger lithium-based salts, such as $LiClO_4$, act as anti-plasticizers and increase the glass transition temperature, through microphase separation and formation of transient crosslinks. However, Galin, et al. [19] showed that the glass transition decreases when LiCl was added to poly[3 – (N,N- diethyl - N- (5 - methacryloyoxy - 3 - oxapentyl) ammonio) propanesulfonate], (called M-2OE-3 in reference 19). These conflicting results suggest that further study is needed on the role of salt addition on the glass transition process.

We present an analysis of the effects of LiCl salt on the thermal and structural properties of the dry state of PZIs having different backbone and side-group chemistries. Three polyzwitterions, shown in Fig. 2, have structures which vary systematically: poly(sulfobetaine methacrylate), PSBMA; poly(sulfobetaine acrylate), PSBA; and, poly(ethyl sulfobetaine methacrylate), PESBMA. PSBMA, shown in Fig. 2a. PSBA (Fig. 2b), is similar to PSBMA, but lacks the methyl group on the backbone, resulting in higher backbone flexibility. PESBMA (Fig. 2c) has the same methacrylate backbone structure as PSBMA, but the quarternary amine groups on the zwitterionic moiety is substituted with ethyl groups instead of methyl groups. These polymers have some similarities to those used by Galin [19], but their polymers had longer side groups.

Our thermal analysis is performed in the region of the glass transition of these materials and is directed toward analyzing this thermal transition to observe the impact of salt addition on the glass transition relaxation process. In 1983, Ten Brinke et al. [21] suggested a way of using thermal analysis to study the effect of crosslinking. They suggested that crosslinks in general could be treated in a manner similar to the crystalline regions in semicrystalline polymers. *I.e.*, crosslinks confine portions of the amorphous phase affecting the thermal properties, such as the glass transition temperature, T_g, the sharpness of the transition, and the transition amplitude, as shown in Fig. 3. The figure shows a sketch of the specific heat capacity, c_p, as a function of temperature, in the vicinity of the glass transition, for a fully amorphous polymer (red trace) and a semicrystalline polymer (blue trace). The less confined amorphous polymer (red) has a lower T_g, a sharper, less broad glass transition temperature range, and larger specific heat capacity increment, $\Delta c_p(T_g)$, compared to the more confined, semicrystalline polymer (blue). Ample evidence exists for this view of semicrystalline polymers and examples of supporting data can be found in references [22–27]. In semicrystalline polymers, the heat capacity increment from the solid state to the liquid state stands as a relative measure of confinement [26]. Through measurement of T_g, its breadth, and heat capacity increment, we are applying the suggestion of Ten Brinke et al. [21] specifically to the dipolar cross-links characterizing our polyzwitterions, with and without added LiCl salt. In chemically crosslinked polymers, previous work has shown that increases in crosslinking density influence the glass transition temperature and the length of the cooperatively re-arranging region [28–34]. We anticipate that with the inclusion of LiCl, the density of the PZI physical crosslinks can be varied, and this would similarly result in changes in the glass transition process.

In support of the thermal property analysis, we also use Wide Angle X-Ray Scattering (WAXS) to determine the average interatomic spacing of PZI-LiCl complexes as a function of added LiCl. Fourier Transform Infrared Spectroscopy (FTIR) is used to determine effects on the absorbance spectra caused by Li^+ and Cl^- ions associating with the zwitterionic moieties in the side groups. Because polyzwitterions are hydrophilic, we develop a procedure to remove bound water, so that the dry solid-state properties of our materials can be studied. Thermogravimetry provides information about the content of the bound water and the onset of thermal degradation as a function of added salt. Finally, carefully dried samples are studied using differential scanning calorimetry (DSC) and its temperature modulated variant, TMDSC in the region of the glass transition. This paper is organized as follows. First the materials and methods are described in Section 2, including the method for water removal, and the calculation of the specific heat capacity from the DSC data. Then, results are presented in Section 3.1-3.2 for X-ray diffraction and infrared absorbance, followed by thermogravimetry in 3.3 and scanning calorimetry in 3.4. Application of the empirical "bead model" of polymers given by Wunderlich [21,22] in Section 3.5 is used to estimate $\Delta c_p(T_g)$, and compare to our experimental data. Conclusions follow in Section 4.

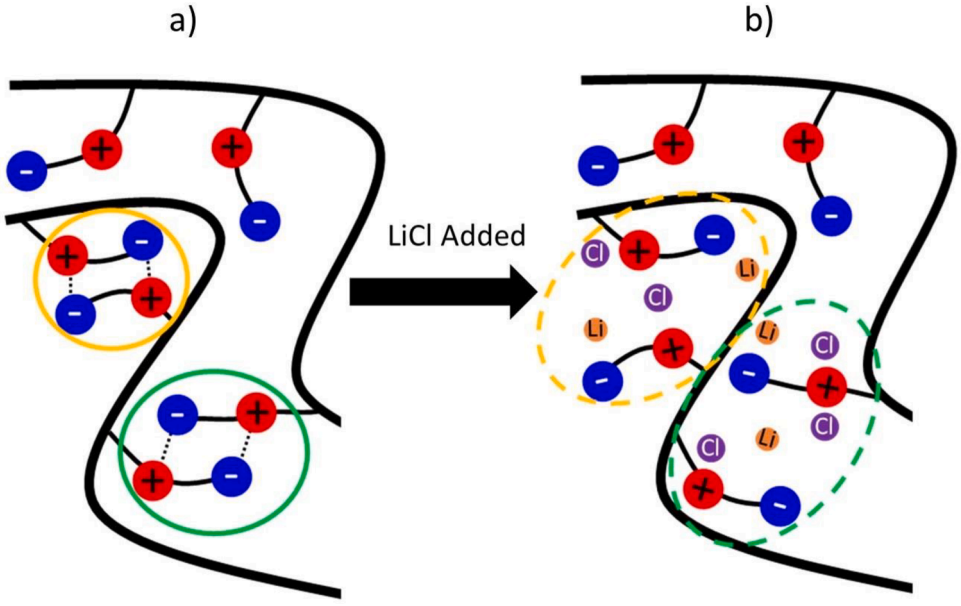

Fig. 1. Structure of PZI with and without salt addition. (a) Polyzwitterion schematic showing intra- and intermolecular crosslinking (yellow and green circles, respectively) of the PZI side groups. (b) PZI with associated salt ions (Li^+, orange; Cl^-, purple) which disrupt both intra- and inter-molecular crosslinking (dashed green and yellow circles, respectively). Adapted from the graphical abstract of reference [20], with permission of the author.

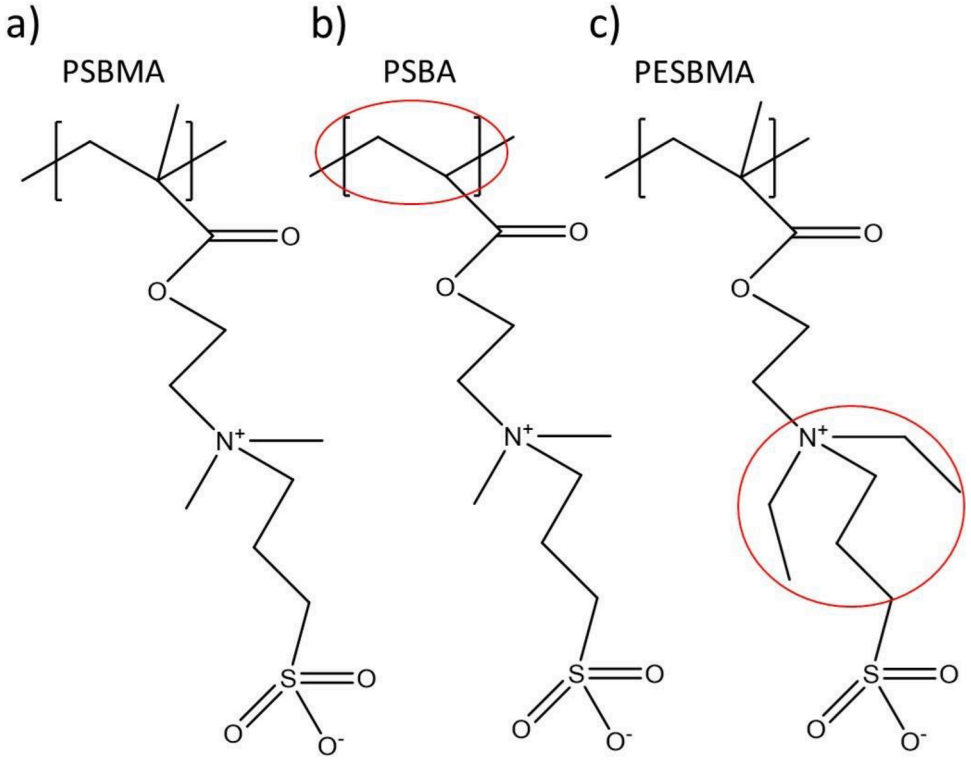

Fig. 2. Monomer units of PZIs based on the sulfobetaine moiety: (a) poly(sulfobetaine methacrylate), PSBMA; (b) poly(sulfobetaine acrylate), PSBA; (c) poly(ethyl sulfobetaine methacrylate), PESBMA. Chemical variations from PSBMA are circled in red.

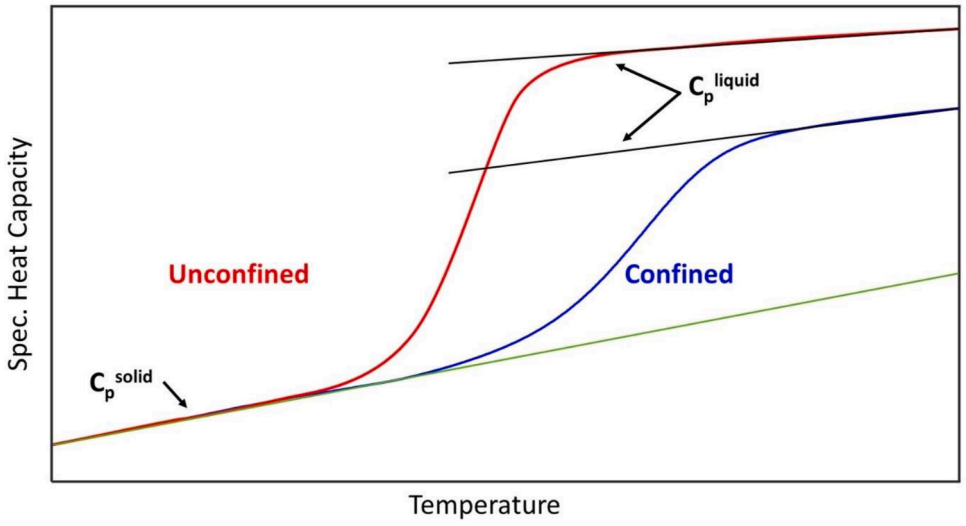

Fig. 3. Sketch of the effects of confinement in a semi-crystalline polymer on the specific heat capacity as a function of temperature, comparing the confined semi-crystalline polymer (blue trace) and the unconfined amorphous polymer (red trace) in the vicinity of the glass transition region. Extrapolated baselines for the solid-state heat capacity (green line) and the liquid-state heat capacities (black lines) highlight changes in the liquid state heat capacity at the glass transition.

2. Materials and methods

2.1. Materials

Monomer synthesis and the polymerization of the PZIs have been reported in previous work [20]. Briefly, the SBMA monomer was purchased from Sigma, whereas SBA and ESBMA were synthesized by the ring opening reaction of 3-propane sultone with the appropriate tertiary amine-containing monomer. The polymers were synthesized using free radical polymerization. CAS numbers for the materials are listed in Supplementary Data Table S1.

Each PZI is dissolved using 2,2,2-trifluoroethanol (Alfa Aesar, Ward Hill, MA, US). Separately, LiCl (Alfa Aesar, Ward Hill, MA, US) is dissolved in DI water. The two solutions are then combined and stirred for 24h at room temperature. Solutions are then drop cast layer by layer to build up thick films. After casting, samples are dried and held in a vacuum oven at room temperature.

The LiCl was added to PZI in various molar ratios with respect to the zwitterionic monomer concentration. We name these complexes as PZI-LiCl. When referring to the salt content, we use 1 mole of ZI monomeric

unit to X moles of LiCl, or 1:X. Polyzwitterions with no added salt are denoted as having a composition of 1:0. PZI-LiCl complexes were prepared in compositions with X ranging from (0.08 - 1.82) ± 1%. Salt concentrations are rounded to ± 1% to account for small variations in weighed mass during measurements. When data are plotted as a function of moles of LiCl per zwitterionic monomer unit, X, the abscissa will be given as "moles of LiCl per mol of ZI". The ZI monomer will be replaced by SBA, SBMA, or ESMBA as needed.

2.2. Characterization methods

Wide angle X-Ray scattering (WAXS) is used to determine the structure of the PZI-LiCl complexes. A Philips PW 1830 X-Ray Generator with a Cu K-α source and a wavelength of $\lambda = 0.1544$nm was used (PANalytical, Almelo, Netherlands). Scattered intensity was measured in $\theta/2\theta$ reflection mode at scattering angles, 2θ, ranging from $2\theta = 5^\circ$ - 45°, with a step scan interval of 0.2°/step and a dwell time of 2s/step. Samples were solution cast into Kapton tape on aluminum holders to create a thick film to enhance scattering. Kapton tape on an aluminum holder was used for background subtraction. Bragg's Law ($n\lambda = 2d\sin\theta$) was applied in first order to determine the average interatomic spacing, d. Noise was smoothed with a Savitzky-Golay filter using a first order polynomial where the frame length used was either 11 or 51. The latter frame length was used to determine the d-spacing from the peak position. The uncertainty in the peak position is determined by the peak range measured using the smaller frame length. This range in peak position is determined for each PZI without added salt and applied to the peak position for the corresponding PZI:LiCl blended complexes.

Infrared absorbance spectra were acquired using a JASCO FTIR-6200 spectrometer (JASCO Instruments, Tokyo, Japan), in attenuated total reflectance mode using a MIRacle KRS-5 diamond crystal (PIKE-Technologies, Madison, WI, US). FTIR spectra were obtained from 400 to 1800 cm^{-1} with a resolution of 4 cm^{-1} with 256 scans co-added after air background subtraction.

Degradation temperatures and bound water content estimates were determined using thermogravimetry (TG) (TGA Q-500, TA Instruments, New Castle, DE, US). We used a heating rate of 20K min^{-1} from room temperature to 1000°C under a dry N_2 purge of 50mL min^{-1}. Sample masses varied from 3 to 10mg and samples were placed directly on the platinum basket. Onset temperature of thermal degradation is determined by the temperature intersection point between the extrapolated mass remaining of the dry undegraded state, and the tangent line to the first degradation step. Variations in baseline selection yielded onset degradation temperature uncertainties of ± 1°C.

Differential scanning calorimetry (DSC) was performed on a DSC Q-100 (TA Instruments, New Castle, DE, US) with an RCS cooler under a dry N_2 purge at 50mL min^{-1}. Heating rates varied from 5 to 20K min^{-1} with sample masses ranging from 3 to 10mg. Samples were heated in the range from −80–250°C. The DSC cell was calibrated using the TZero calibration method in which heat capacity is calibrated using a sapphire standard, and the heat flow rate and temperature are calibrated using an indium standard.

A "Ratchet Method" was developed to remove both surface and molecularly bound water as is shown in Fig. 4a. Samples are heated at a rate of 20K min^{-1} from 0°C to 100°C and then cooled to 0°C at 20K min^{-1}. The samples are then heated to 120°C and cooled back to 0°C. This is repeated to higher and higher temperatures until the glass transition is reached. After undergoing the glass transition, the sample is cooled and then heated and cooled three times above T_g to ensure the dry state has been achieved. Our polyzwitterions must have their bound

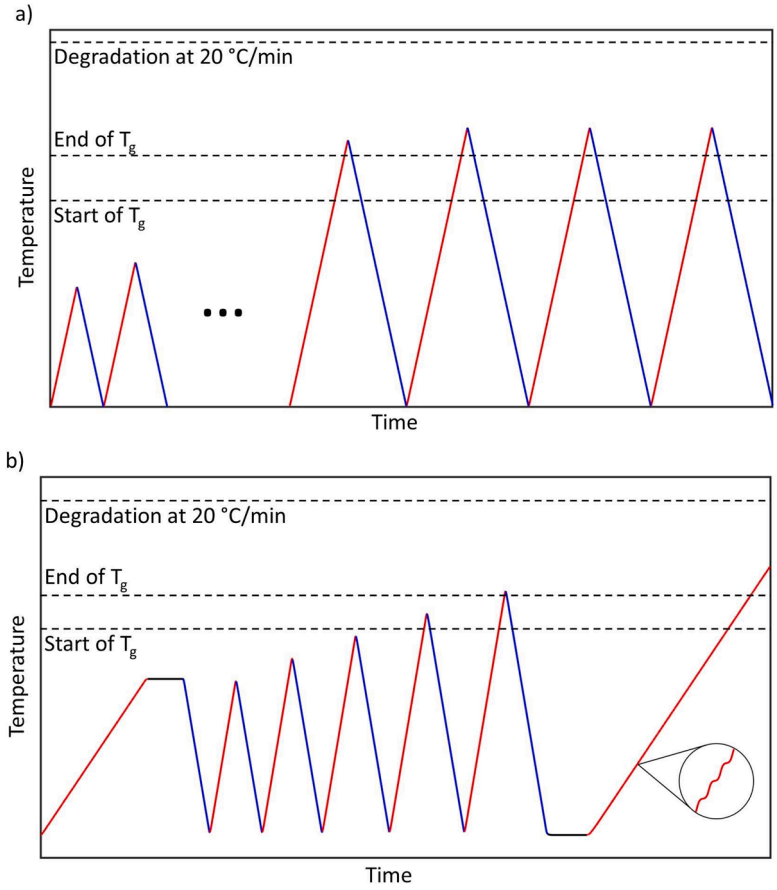

Fig. 4. (a) Ratchet method for DSC showing the temperature/time profile for successively heating to higher temperatures. (b) Modified ratchet method for TMDSC. Inset shows the magnified view of the final method segment which includes temperature modulation.

water removed in situ, inside the DSC cell. These materials pick up water very readily, and it is efficient to use the rachet method to remove bound water immediately prior to the final DSC scan to high temperature. In prior work, the absence of water was studied through thermogravimetry and DSC by Clark, et al. [35] using a "quasi-isothermal" procedure. Here the PZI samples (including the three PZIs used in the present study) were heated to 160°C followed by a 20-minute isothermal hold. Following this hold, the temperature was incrementally increased by 2°C followed by a 20-minute isothermal hold until 240°C was reached. During the isothermal holding periods, the PZI mass did not change; mass was stable until the onset of degradation. In our work after the ratchet method, the samples were heated three times to a temperature greater than T_g. There was no shift in the solid-state heat capacity which indicates no mass was lost (either to water removal or through degradation). Then, after the final heating, the glass transition temperature of the sample in its dry, water-free state was determined using the Moynihan method [36]. Glass transition temperatures are reported with an uncertainty of ± 1°C as determined by small perturbations in baseline selections for both the solid and liquid state extrapolations used in the Moynihan method.

Temperature Modulated DSC (TMDSC) was performed on the same DSC Q-100 with the same purge conditions. Determination of the heat capacity increment at T_g was performed using the three runs method, each run following an iso-ramp-iso protocol: 10min isothermal hold, then ramping at 5K min^{-1} with temperature modulation of ±0.796K min-^{1} and period of 60s, followed by a 10min isothermal hold. For the three runs method, the iso-ramp-iso segment is performed on an empty aluminum reference, then on a sapphire standard, and finally on the sample. All samples are contained in Al pans and lids, so Al serves as a common background whose effect is removed in the three-runs method. The iso-ramp-iso segment is performed following a modified ratchet method shown in Fig. 4b. The method begins with an initial heating ramp at 5K min^{-1} to 140°C and a 10min isothermal hold. This isothermal segment was added as a precautionary step to slowly eject water, since too-rapid removal of water during fast heating can cause polymer "popcorning" through rapid volume expansion. This popcorning changes the quality of thermal contact inside the DSC pan and can even dislodge the sample from the heater. Once bulk water is driven off, we use a standard ratchet method, heating only once through the glass transition. After the start and end of the glass transition are seen (second to last heating segment in Fig. 4b), the sample is cooled and reheated using the iso-ramp segment to complete the third stage of the three runs method.

2.3. Method for determining the specific heat capacity

The three-runs method is used in TMDSC to determine the specific heat capacity of an unknown material by scaling against the measured specific heat capacity of a known refence material, in this case sapphire. In the usual manner, specific heat capacity in units of J g^{-1} K^{-1} is denoted by lower case c, while heat capacity in units of J K^{-1} is denoted by upper case C. The measured specific reversing heat capacity of the sapphire, $c_p^{Spph\text{-}meas}$ is determined by subtracting the TMDSC reversing heat flow rate of the aluminum background, HF^{Al}, from the sapphire reversing heat flow rate, HF^{Spph}, and dividing by the mass of the sapphire, m_{Spph}, and the heating rate, β, shown in Eq. (1):

$$c_p^{Spph-meas}(T) = \frac{1}{m_{Spph}\,\beta}\left(HF_{Spph}(T) - HF_{Al}(T)\right) \tag{1}$$

The measured specific reversing heat capacity of sapphire is then compared to the literature values of sapphire, $c_p^{Spph\text{-}Lit}$, from NIST [37]. This gives the scaling factor, K in Eq. (2), which can be used to scale the measured specific heat capacity of a sample by comparison to the well-known properties of sapphire:

$$K(T) = c_p^{Spph-Lit}(T) \Big/ c_p^{Spph-Meas}(T) \tag{2}$$

Using this scaling factor, the total specific reversing heat capacity of the PZI-LiCl complex, c_p^{Comp}, can be determined from Eq. (3):

$$c_p^{Comp}(T) = \frac{1}{m_{Comp}\,\beta}\left(HF^{Comp}(T) - HF^{Al}(T)\right)K(T) \tag{3}$$

where m_{Comp} is the final dry mass of the polymer plus salt, after all water has been removed. Following our calibration protocol, the uncertainty in the total specific reversing heat capacity is ± 2%, as reported by TA Instruments. Since PZI-LiCl complexes tend to absorb water, in the next section we derive the equations needed to determine the final dry mass of polyzwitterion plus salt.

2.4. Method for determining the mass of the polyzwitterion-salt complex

The purpose of this section is to derive an expression for the final mass, m_{Comp}, of the polyzwitterion-salt complex after it has been dried free of bound water. The general procedure is as follows. The sample is heated first when it is wet. Its initial mass, m_i, is the sum of the mass of the polyzwitterion-salt complex and the mass of water: $m_i = m_{Comp} + m_{Water}$. Then the Rachet Method drying process removes the water, and afterwards the sample is heated again when it is dry, at which point its dry mass, m_{Comp}, is determined. The heat flow rates at room temperature (25°C) are compared in the wet and dry scans, allowing m_{Water}, and hence m_{Comp}, to be determined. Once the mass of the polyzwitterion-salt complex is known, the measured heat capacity can be converted to the *specific* heat capacity as derived in Eq. (3).

In the initial heating, we assume that the total heat flow rate, HF_i^{Total}, comprises the heat flow rates from the dry polyzwitterion-salt complex, HF^{Comp}, and from the water, HF^{Water} as indicated in Eq. (4a). Eq. (4b) substitutes the specific heat capacity in J g^{-1} K^{-1}, times the mass, times the heating rate in K s^{-1}, for the heat flow rate which is in J s^{-1} [38]:

$$HF_i^{Total}(T_1) = HF_i^{Comp}(T_1) + HF_i^{Water}(T_1) \tag{4a}$$

$$HF_i^{Total}(T_1) = m_{Comp}c_p^{Comp}(T_1)\beta_i + m_{Water}c_p^{Water}(T_1)\beta_i \tag{4b}$$

where m_{Comp} and m_{Water} are the mass of the dry polyzwitterion-salt complex and the water, respectively, and $m_{Comp} + m_{Water} = m_i$, the initial mass. The initial scan's heating rate is b_i. HF^{Comp} is the combined heat flow rate of the PZI and the $Li^+$and Cl^-. The heat flow rates in Eqs. (4a,4b) are temperature dependent and in our case, we evaluate them at T_1, which is taken to be 25°C on the initial heating since no water has been evaporated at this point.

As heating continues during the Rachet Method, water is removed, and the mass of water decreases. Because of the variable nature of the interaction of the Li^+ and Cl^- ions in the polyzwitterion-salt complex, the heat flow rate (the first term on the right-hand side of Eq. (4b)) was not further separated into its individual components of the polyzwitterion and the salt.

After the Ratchet Method has finished, and all bound water has been removed, the sample is heated again. HF_f^{Total}, taken at a temperature T_2 (25°C) now comprises the heat flow rate due solely to the polyzwitterion-salt complex:

$$HF_f^{Total}(T_2) = m_{Comp}c_p^{Comp}(T_2)\beta_f \tag{5}$$

Combining Eqs. (4b) and (5) we develop an expression for the mass of water lost through the drying process, m_{Water}. The final polymer mass, m_{Comp}, can be determined by taking the difference between the initial total mass, m_i, and the initial mass of the water, m_{water}. The latter quantity is determined using Eq. (6) which relates the total initial heat flow rate, HF_i^{Total}, to the final total heat flow rate, HF_f^{Total}, and the specific heat capacity contribution of water, c_p^{water}, known from literature [39]:

$$HF_i^{Total}(T_1) = HF_f^{Total}(T_2)\frac{\beta_i}{\beta_f} + m_{water}c_p^{water}(T_1)\beta_i \quad (6)$$

$$m_{Water} = \frac{1}{C_p^{Water}}\left(\left|\frac{HF_i(T_1)}{\beta_i}\right| - \left|\frac{HF_f(T_2)}{\beta_f}\right|\right) \quad (7)$$

$$m_{Comp} = m_i - m_{Water} \quad (8)$$

where the final scan's heating rate is b_f. Once the dry mass of the polyzwitterion-salt complex, m_{Comp}, is known the total specific reversing heat capacity of the complex can be determined using Eq. (3).

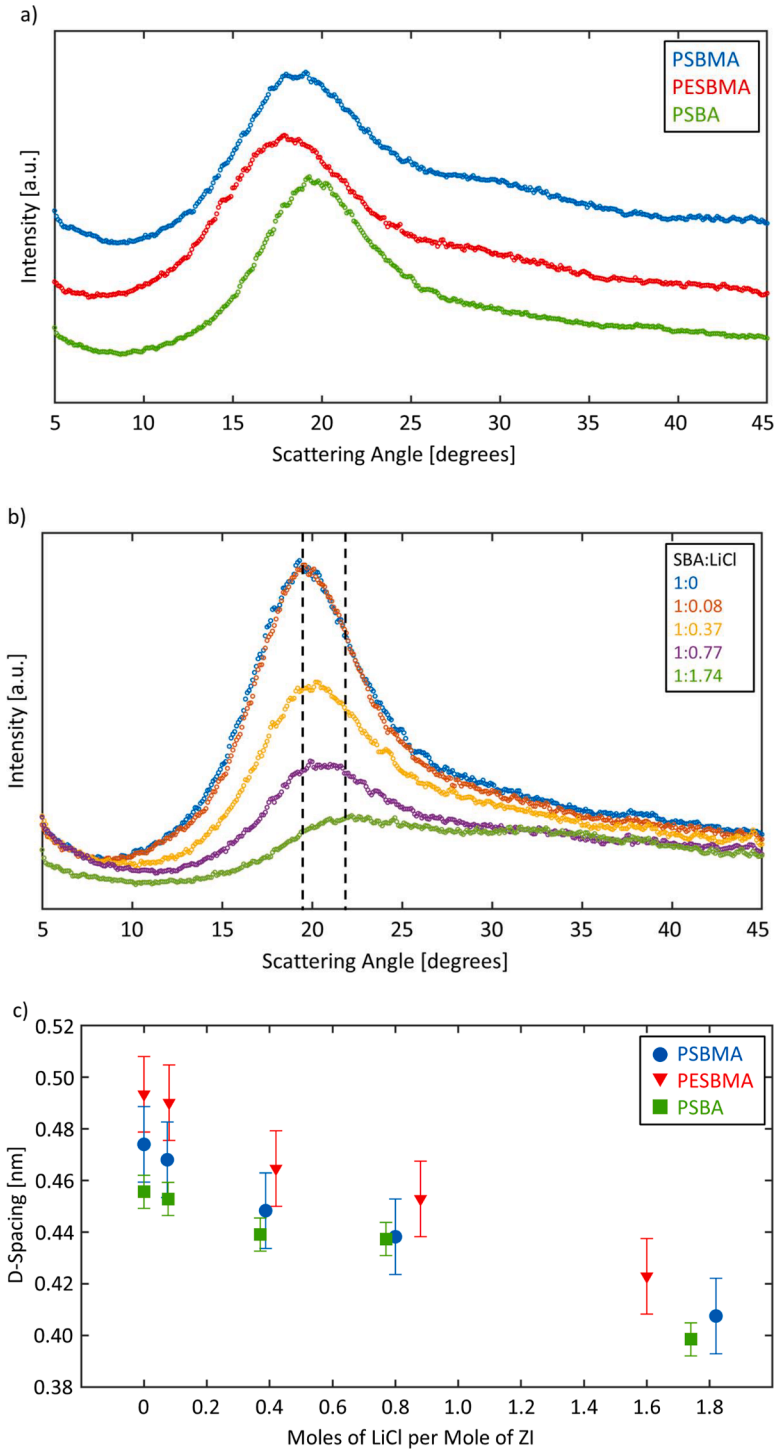

Fig. 5. (a,b) WAXS intensity vs. scattering angle, 2q for: (a) PSBMA (top blue curve), PESBA (middle red curve), and PSBA (bottom green curve); (b) PSBA-LiCl complexes with molar salt content ranging from SBA:LiCl 1:0 (top blue curve), to highest salt content, 1:1.74 (bottom green curve). Black dashed lines are guides to the eye highlighting peak shift to higher scattering angles as salt content increases. (c) Average D-spacing for all polyzwitterion-LiCl complexes as a function of molar salt content.

3. Results and discussion

3.1. Salt addition affects interatomic spacing

Wide Angle X-Ray Scattering (WAXS) intensity vs. scattering angle, 2θ, for PZIs and for PSBA-LiCl complexes are shown in Fig. 5a, b, respectively. Effects of salt on the WAXS scans of the other PZIs are shown in supplementary Fig. S1. In Fig. 5a we see broad intensity curves without sharp crystalline reflections for all three PZIs indicating that they are fully amorphous. For PSBMA (top blue curve), the amorphous peak occurs at a scattering angle of 18.70±0.57°. With the changes made to the side group through the addition of the ethyl groups in PESBMA (middle red curve) the peak maximum is shifted leftward to 17.96±0.42°. This is an indication the interatomic spacing has increased, which likely results from the bulkier side group. In PSBA (bottom green curve) the amorphous peak maximum is shifted rightward to a higher scattering angle of 19.3±0.28° indicating more dense chain packing caused by absence of the methyl group in the backbone.

Polyzwitterions form dipolar cross links and with the addition of LiCl there is an interruption of this side chains cross-linking. The effect of salt addition on PSBA can be seen in Fig. 5b. As salt content increases, the curves become broader and less intense, and the position of the peak maximum shifts to higher scattering angles. No LiCl crystals are seen in the PSBA-LiCl complexes (no sharp diffraction peaks), even when the LiCl content increase above the 1:1 molar ratio of SBA:LiCl. These observations about peak breadth, intensity, and position are similar in all the PZIs (see supplementary Fig. S1 for data on PSBMA-LiCl and PESBMA-LiCl complexes).

The measured d-spacings for all three PZIs with and without salt are shown in Fig. 5c. As LiCl content increases there is a consistent decrease in d-spacing of the peak maximum. Without salt, the dipolar crosslinks lock the polyzwitterion into a confined structure with larger average interatomic spacing. The disruption of crosslinking reduces the intermolecular spacing as the $Li^+$and Cl^- ions associate with the charges on the side group. Reduction of d-spacing is evidence in support of the view that disruption of crosslinking occurs upon salt addition. The general trends seen in the PZIs without salt (Fig. 5a) are also see in the PZI-LiCl complexes (Fig. 5c) viz., the d-spacings appear in the same order: $d_{PSBA}(= 0.456\pm0.006nm) < d_{PSBMA} (= 0.474\pm0.015nm) < d_{PESBMA} (= 0.493\pm0.011nm)$. Thus, we conclude that the changes in the d-spacing of the peak maximum are dominated by chemical variations of the monomers, and these persist even in the presence of LiCl salt. The effect of salt addition is to systematically reduce the d-spacing below that of the salt-free polyzwitterion.

3.2. Salt ions associate with PZI side groups

Differences in the chemical structure and side group interactions of the three polyzwitterions were observed using Fourier transform infrared spectroscopy (FTIR). In Fig. 6a the absorbance vs. frequency for PSBMA (top blue curve), PESBMA (middle red curve), and PSBA (bottom green curve) are compared. Individual absorbance spectra were normalized to the peak intensity of the $C{=}O$ peak at 1726 cm^{-1} (red dotted line) [40]. This peak, common to all three PZIs, was chosen as the

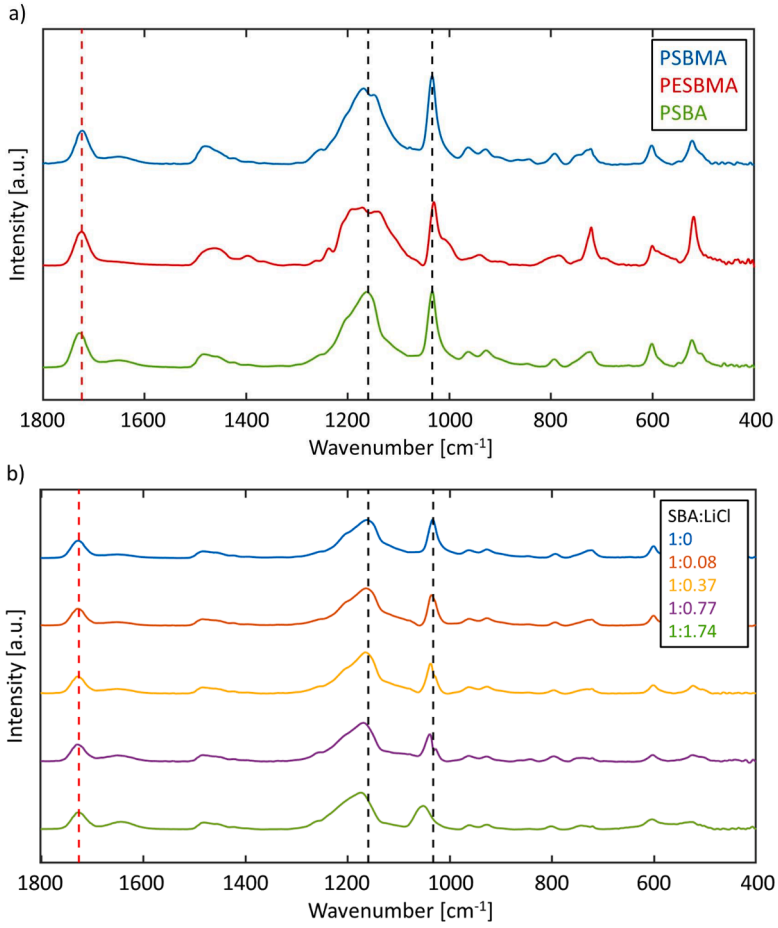

Fig. 6. Normalized FTIR absorbance vs. frequency for: (a) PSBMA (top blue curve), PESBMA (middle red curve), and PSBA (bottom green curve); (b) PSBA-LiCl complexes. Spectra range from molar salt content of SBA:LiCl 1:0 (top blue curve) to high salt content in the 1:1.74 (bottom green curve). $C{=}O$ peak at 1726 cm^{-1} (red dotted line) is used for peak intensity normalization. Shifts in $S{=}O$ symmetric (1032 cm^{-1}) and asymmetric (1160 cm^{-1}) stretching vibrations (black dotted lines) highlight Li^+ion association shifts. Curves are shifted vertically for clarity.

normalization peak since we observed no changes in peak position or shape in this spectral region as a function of chemical composition or salt content. Peaks at 1032 cm^{-1} and 1160 cm^{-1}, marked by black dotted lines, are the symmetric and asymmetric stretching vibrations, respectively, of the *S=O* bond [40]. In PESBMA (red), both the 1160 cm^{-1} and the 1032 cm^{-1} peaks becomes broader compared to PSBMA (blue). The addition of the ethyl groups on the side group of PESBMA results in a broader distribution of vibrational frequencies of the *S=O* group at the end of the side group. Increase in the absorbance of the 720 cm^{-1} peak (CH_2 rocking) in PESBMA (red) compared to PSBMA (blue) is due to the increase in the number of CH_2 bonds in the side group.

In Fig. 6b five spectra for PSBA-LiCl complexes are shown, ranging from the PSBA with molar salt content of SBA:LiCl 1:0 (no salt, top blue curve) to the highest salt content of 1:1.74 (bottom green curve). As LiCl content increases, the frequency of the *S=O* vibration shifts to higher wavenumbers in both the 1032 cm^{-1} (*sym*) and 1160 cm^{-1} (*asym*) peaks. The symmetric *S=O* vibration in PSBA:LiCl complexes shifts to 1052 cm^{-1}, and the asymmetric vibration shifts to 1174 cm^{-1}. At the highest salt content, the 1032 cm^{-1} symmetric stretching vibration broadens and decreases in amplitude compared to its asymmetric counterpart. This shift in the *S=O* peak is caused by association of Li^+ ions on the terminal end of the side group, and it is notable that this effect is seen for excess salt content, i.e., when the molar salt content exceeds 1:1 ZI:LiCl. This result was seen also in PSBMA and PESBMA. Spectra for these complexes are shown in the supplemental Fig. S2.

3.3. Salt affects degradation and bound water content

Due to the hydrophilic and hygroscopic nature of both the PZIs and LiCl, PZI-LiCl complexes contain a large amount of bound water. Using thermogravimetry, an initial estimate for bound water content and the onset of thermal degradation can be determined. Fig. 7a shows the degradation profile for PSBA-LiCl complexes with molar salt content ranging from SBA:LiCl 1:0 (no salt, blue curve) to the highest salt content, 1:1.74 (green curve). Complete degradation of the neat PZI polymer was observed once the temperature reached 1000°C, as show in Figs. 7a and Supplementary Fig. S3a, b. Complete degradation of crystalline LiCl salt was also seen at 1000°C and these data are presented in Supplementary Fig. S3c. However, in the case of the PZI-salt complexes, we observed some residual mass remaining at 1000°C due to sticky char. This char could reflect the interaction between LiCl and degradation products of the PZI. The individual curves are reported as the percent of PZI-LiCl complex mass remaining.

The first step change seen around 150°C is the ejection of bound water which can continue to temperatures as high as 250°C. The first step in water removal, occurring from 25 to 150°C, is the removal of surface bound water (freezable bound water, in the categorization of McGrath [41]). The second step seen ranging from ~150–250°C is the ejection of non-freezing molecularly bound water [41] which requires greater energy to effect its release. Water content in PSBA and PSBA-LiCl complexes ranges from 1wt.% in the polyzwitterion without salt, to 20wt.% in the 1:1.74 sample. The third degradation step starting around 270°C is the pyrolysis of the polymer chain which leaves behind a

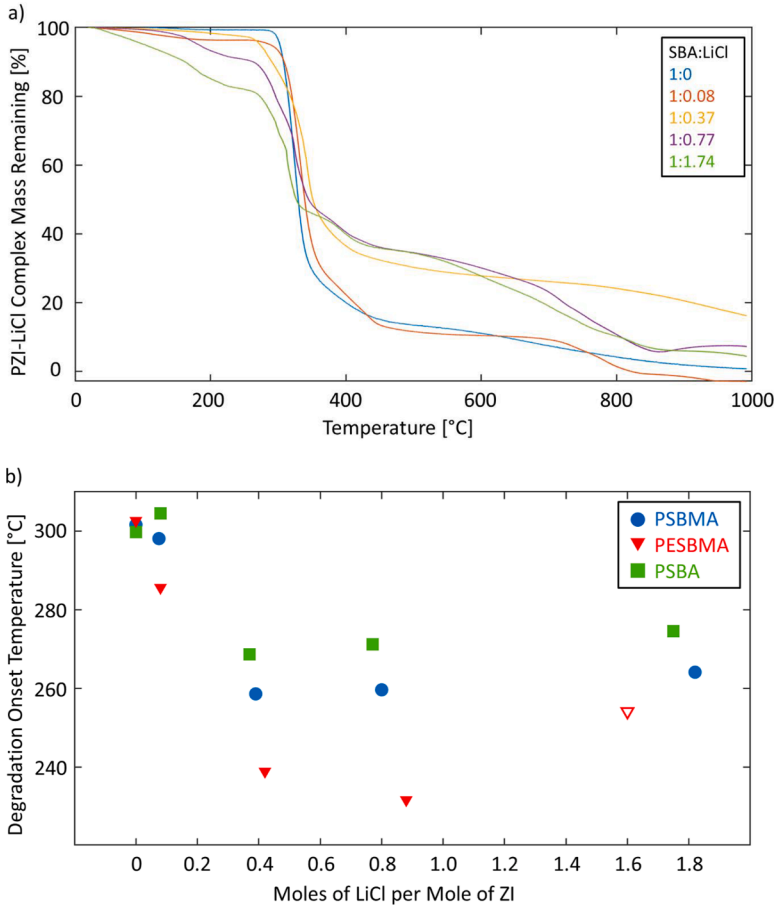

Fig. 7. (a) Thermogravimetric analysis of PZI-LiCl complex mass remaining vs. temperature for PSBA-LiCl complexes, with molar salt content ranging from SBA:LiCl 1:0 (no salt, blue curve) to high salt content 1:1.74 (green curve). Water loss is shown by the first step around 150°C followed by the first stage in degradation around 300°C. (b) Onset temperature of thermal degradation as a function of molar salt content for PSBMA (blue circles), PESBMA (red triangles), and PSBA (green squares). Open red triangle for PESBMA refers to a sample which underwent rapid thermal expansion ("popcorning") during heating.

carbon residue [10]. The higher temperature degradation around 450–600°C is typically attributed to breakdown of the carbon residue [10]. All PZI-LiCl complexes showed similar trends, and degradation profiles are shown for PESBMA, PSBMA, and crystalline LiCl salt in Supplementary Fig. S3a,b,c, respectively. LiCl salt showed complete loss of mass by 1000°C caused by the evaporation of molten LiCl.

Onset temperatures of thermal degradation as a function of LiCl content are shown in Fig. 7b. We suggest that as the salt content increases, the onset of degradation occurs at progressively lower temperatures because of increased disruption of the dipolar crosslinking. When the complex is electrostatically highly crosslinked, which is the case for both the polyzwitterion without salt and the complexes with low salt content, there is a hindrance of chain mobility. Reduced mobility in the side chain helps stabilize the PZI against thermal degradation [10]. PESBMA-LiCl complex with molar salt content of ESBMA:LiCl 1:1.6 (open red triangle) is an outlier. This sample had the largest water content and experienced rapid volume expansion ("popcorning") during TG tests under fast heating conditions (20K min^{-1}), and an example is shown in Supplementary Fig. S4. With this one exception, as the dipolar crosslinking is disrupted by increasing salt addition, thermal stability decreases as a function of increase in salt content [11]. Table 1 lists the onset temperatures of degradation for the polyzwitterions without salt, and for the PZI-salt complexes with the lowest degradation temperatures. Upon salt addition, the change in degradation onset temperature between the polyzwitterion without salt, and the PZI-salt complex with the lowest degradation onset, follows the trend: $\Delta T_{d,PESBMA}$ (= 71±1K) > $\Delta T_{d,PSBMA}$ (= 43±1K) > $\Delta T_{d,PSBA}$ (= 32±1K). The thermal stability of PESBMA is reduced the most, and thermal stability of PSBA is reduced the least, upon salt addition.

3.4. Bound water plasticizes the glass transition

Bound water is known to plasticize polymers and decrease the glass transition temperature through chain lubrication, which adds high mobility into the system [42,43]. To determine the effects of changes in monomer chemistry and the association of LiCl on the side groups, bound water must be removed. Conventional drying methods, such as heating above the glass transition and holding in the liquid state, cannot be used with our PZIs, because they have relatively low degradation temperatures relative to their high glass transition temperatures [20]. To avoid degradation during water removal, we use the Rachet Method described earlier.

The Rachet Method is demonstrated for PSBA-LiCl complex with molar salt content of SBA:LiCl 1:0.08 in Fig. 8a. The first heating is used to drive off surface water which can be seen by the endothermic event (downward deflection from the baseline) beginning at 40°C. This endothermic event reflects contributions from both the plasticized glass transition process and from the water removal. Successive heating scans to higher temperatures show that this thermal event shifts to higher temperatures (at around 90°C in the second heating) as more water is removed on each cycle. As water is driven off, the solid-state baseline shifts upward to higher values, as indicated in Fig. 8a by the red dotted lines. The shift in solid-state baseline is due to the loss of mass attributed to the ejection of water. Fast heating and cooling (20K min^{-1}) allows for the removal of water while spending minimal time at high temperatures, thus reducing the chance of early onset of degradation. At the completion of the Rachet Method, the final dry-state glass transition is measured using the Moynihan method [36].

Fig. 8b shows the glass transition temperatures of the dry PZI-LiCl complexes as a function of molar salt content: PSBMA-LiCl (blue circles), PSBA-LiCl (green squares), and PESBMA-LiCl (red triangles). The red box highlights the three polyzwitterions with no added salt. PZIs without LiCl have glass transition temperatures, T_g, increasing in the order: $T_{g,PSBA}$(= 200±1°C) < $T_{g,PESBMA}$ (= 204±1°C) < $T_{g,PSBMA}$ (= 237±1°C). PESBMA and PSBA have very similar glass transition temperatures that are lower than that of PSBMA by 33±1 and 37±1K, respectively. Both chemical variations, the absence of the methyl group in the backbone for PSBA and the presence of the ethyl groups to the side group for PESBMA, led to a lower glass transition temperature compared to that of PSBMA. This is due to the higher flexibility of the backbone in the case of PSBA. In PESBMA the bulkier side group adds rigidity to the side group, hindering the formation of dipolar crosslinks which also adds mobility to the system and reduces the glass transition temperature.

For all PZI-LiCl complexes, as LiCl content increases, there is an overall decrease in the glass transition temperature until a plateau is reached at a molar salt content of ZI:LiCl ~1:0.8. The steepness of the change from the largest value of T_g (that of the polyzwitterions without salt) varies with chemical structure of the monomer unit. The difference, ΔT_g, between the largest and smallest values of T_g ($\Delta T_g = T_g - T_g^{min}$) indicates the effect of adding salt and these values are also shown in Table 1. The change in T_g follows the sequence: $\Delta T_{g,PSBMA}$ (= 62±1K) > $\Delta T_{g,PSBA}$ (= 43±1°C) > $\Delta T_{g,PESBMA}$ (= 29±1K). LiCl is shown to be a plasticizer for all three PZIs. Due to the low molecular size and anion polarizability, the probability of forming a covalent bond is reduced leading to a lower likelihood of the forming microphase separations at high molar salt ratios. For all high molar salt ratios (≥1:1), we observed no crystalline peaks in WAXS that would be a signature of phase separation of the LiCl into crystalline regions.

The impact of salt addition on the glass transition is quite strong in PSBMA, and much less so in PESBMA. The glass transition drops as much as 62±1K in PSBMA upon addition of salt, while PESBMA T_g is lowered only by 29±1K. Competing effects are responsible for these trends. First, PSBMA polyzwitterion without salt has the highest T_g because its backbone is more rigid than that of PSBA, and its ability to form dipolar crosslinking is very strong compared to PESBMA given the smaller overall diameter of the side group which improves chain packing. When salt is added to PSBMA, it affects side group packing and crosslinking ability, but not the backbone rigidity. This dramatically decreases T_g in PSBMA.

PESBMA experiences a much smaller impact of salt addition on its T_g. The presence of the two ethyl groups to the side group of PESBMA hinders the side group flexibility and packing more than the methyl groups on PSBMA. It also reduces the tendency to form dipolar crosslinks even in the polyzwitterion without salt. This is supported by the very large reduction in thermal stability in PESBMA compared to the other two polyzwitterions. Onset of degradation drops by 72±1K with added salt. With the addition of LiCl further disruption of these crosslinks reduces the glass transition to a value of 175±1°C.

In PSBA the absence of the methyl group in the backbone leads to higher mobility into the system through increased backbone flexibility,

Table 1
Temperatures of the glass transition, T_g, and degradation onset, T_d, of polyzwitterions without salt, and their changes upon LiCl addition.

PZI	T_g [a] ± 1°C	T_g^{min} [b] ± 1°C	ΔT_g [c] ± 1 K	T_d [d] ± 1°C	T_d^{min} [e] ± 1°C	ΔT_d [f] ± 1 K
PSBMA	237	175	62	301	258	43
PESBMA	204	175	29	302	231	72
PSBA	200	157	43	300	268	32

[a] Glass transition temperatures of the polyzwitterion without salt, determined by the Moynihan method [17] from DSC heat flow data taken at heating rate of 20K min^{-1} after cooling at rate of 20K min^{-1}.
[b] Glass transition temperature of the salt-containing complex having the lowest value of T_g, determined as in (a).
[c] Difference between T_g and T_g^{min}.
[d] Degradation onset temperatures of polyzwitterions without salt, determined by TG during heating at 20K min^{-1}.
[e] Degradation onset temperatures of the salt-containing complex having the lowest value of T_d, determined as in (d).
[f] Difference between T_d and T_d^{min}.

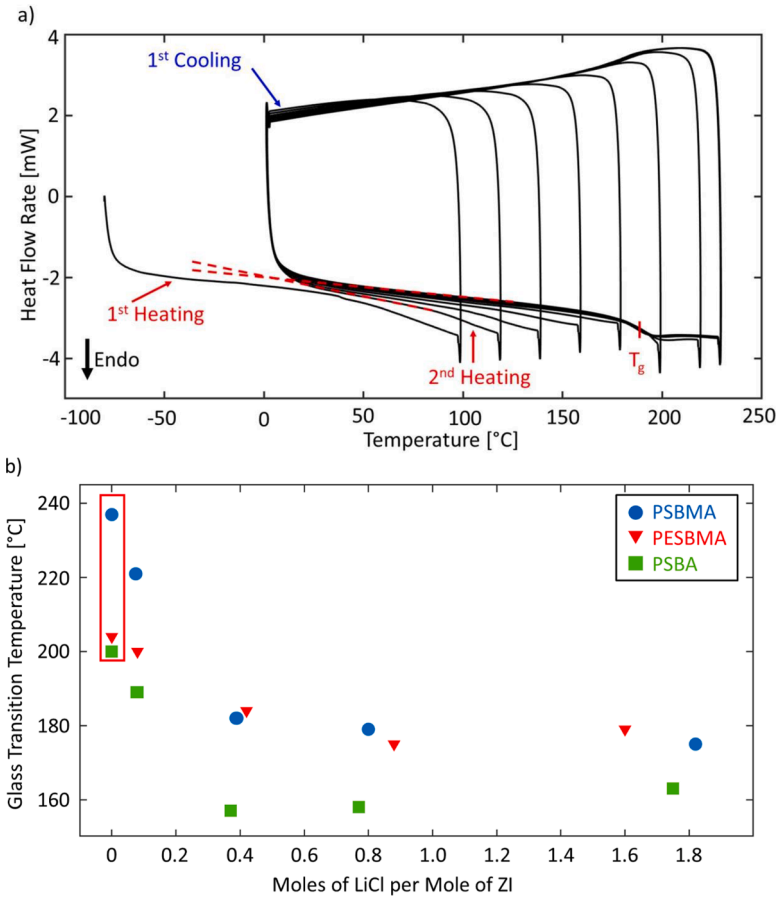

Fig. 8. (a) Heat flow rate as a function of temperature for the PSBA-LiCl complex, at molar salt content of SBA:LiCl 1:0.08 showing use of the Ratchet Method for water removal. Red dotted lines show the shift in solid-state heat flow rate indicative of mass loss between the 2nd and 6th scans. Solid red line marks the glass transition temperature, T_g, determined using the Moynihan Method [36]. (b) Glass transition temperature as a function of molar salt content for polyzwitterion-LiCl complexes. Red box highlights change in T_g due to differences in the chemical structure under conditions of no salt addition.

which could reduce the number of crosslinks formed in the polyzwitterion without salt. Both PSBA and PESBMA however show a much lower ΔT_g than in PSBMA, since these two polyzwitterions already have a large percentage of possible crosslinks disrupted through their chemical structure variations from PSBMA. PSBMA has both the highest T_g and greatest ΔT_g.

3.5. Salt addition reduces molecular confinement

Using TMDSC, high precision solid and liquid state heat capacities were able to be measured for the PSBA-LiCl complexes. Following the modified Ratchet Method shown in Fig. 4b for water removal, the specific reversing heat capacities [43–45], $c_p^{Comp}(T)$, of PSBA-LiCl complexes were evaluated using Eq. (3). Fig. 9a shows the results for complexes with molar salt contents ranging from SBA:LiCl 1:0–1:1.5. Individual curves are shifted on the y-axis to align all curves at a fixed point, 100°C, for ease of comparison. Since LiCl has no thermal features in the temperature range in which the PZI glass transition is occurring [46], the heat capacity increment at T_g is attributed solely to the polyzwitterion. Therefore, the effects shown in Fig. 9 are attributable to the polyzwitterion component of the PSBA-LiCl complexes. There is a general reduction in the glass transition temperature and an increase in the liquid state heat capacity (as shown in Fig. 9b). The breadth of transition increases slightly as a function of increase in the salt content.

T_g was determined using the Moynihan method of equal areas [36]. In our case, T_g is equal to the fictive temperature since there is no physical aging present. As LiCl content increases there is an initial decrease in T_g, which then reaches a plateau at a molar salt content of SBA:LiCl 1:0.77. It has been reported that the high charge density of Li^+ it is able to associate with multiple counter ions [47]. This would mean that the free Li^+ ions could associate onto multiple neighboring side groups, disrupting the intra- and interchain dipolar crosslinking. A reduction in crosslinking would increase the mobility of the polyzwitterion chains, as seen in Fig. 9b, lowering the glass transition temperature from 197±1°C in the polyzwitterion without salt, to 158±1°C in the 1:0.77 complex. The T_g values are reported in Table 2.

The heat capacity increment is defined as the difference between the heat capacities of the extrapolated liquid-state baseline and the extrapolated solid-state baseline, evaluated at T_g as shown in Eq. (9):

$$\Delta c_p(T_g) = c_p^{liquid}(T_g) - c_p^{solid}(T_g) \quad (9)$$

A graphical example is presented in supplementary Fig. S5. The heat capacity increment is also affected by the salt content. In Fig. 9b, as LiCl content increases, $\Delta c_p(T_g)$ first increases and then reaches a plateau (values are listed in Table 2) indicative of a less confined polymer state in the presence of salt. As mentioned in the Introduction, dipolar crosslinking may impose restrictions to molecular mobility similar to that which is seen in semi-crystalline polymers. In the latter case, as the rigid fraction (provided by the crystals, or by the rigid amorphous fraction), decreases and the mobile amorphous fraction concomitantly increases, the glass transition temperature is reduced, the breadth of the transition is reduced, and the heat capacity increment at T_g is increased [22–27]. The crystalline/rigid domains confine the mobile amorphous polymer chains causing the glass transition temperature to increase; when those domains are removed, T_g is reduced, and the liquid state heat capacity increases (which drives the increase in $\Delta c_p(T_g)$). This same

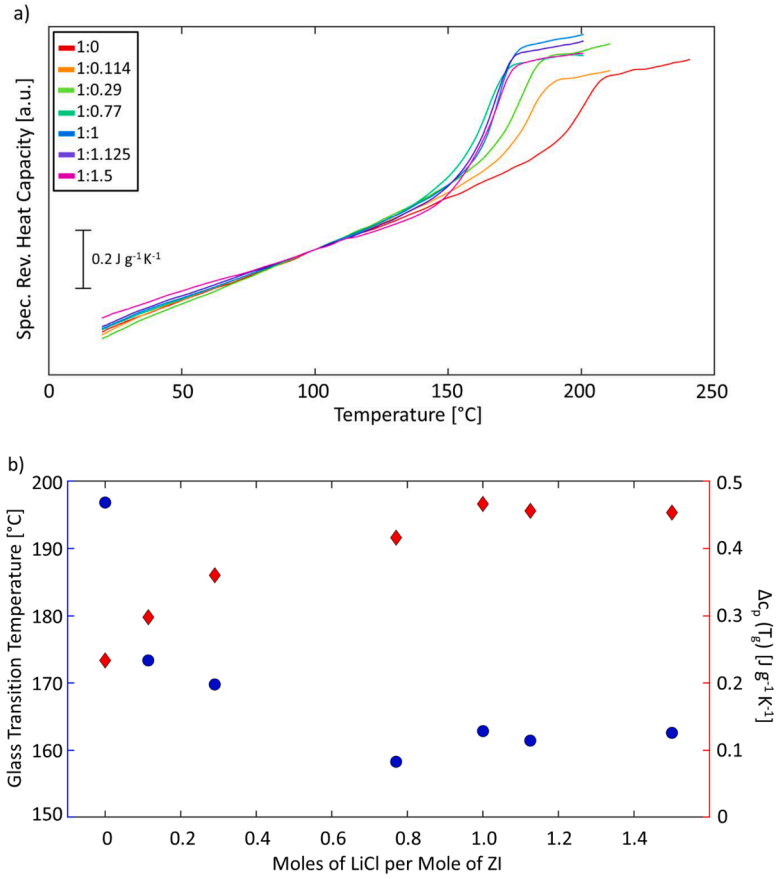

Fig. 9. (a) Specific reversing heat capacity, $c_p^{rev}(T)$, as a function of temperature for PSBA-LiCl complexes at the molar salt contents, ZI:LiCl, as indicated. Curves have been vertically shifted to aid in comparison. (b) The glass transition temperature (left axis, blue circles) and heat capacity increment at T_g, $\Delta c_p(T_g)$ (right axis, red diamonds) as a function of salt content for PSBA-LiCl complexes for data presented in (a).

Table 2
Glass transition temperature and specific heat capacity increment of PSBA-LiCl complexes as a function of LiCl content.

SBA:LiCl, mol/mol	$T_g \pm 1$, °C	$\Delta c_p(T_g) \pm 2\%$, J g^{-1} K^{-1}	$\Delta c_p(T_g) \pm 2\%$ [a], J mol^{-1} K^{-1}	$\Delta c_p(T_g)$ / Δc_p^{bead} [b]
1:0	197	0.23	67.94	0.51
1:0.114	173	0.30	88.62	0.67
1:0.29	170	0.36	106.34	0.81
1:0.77	158	0.42	124.06	0.94
1:1	163	0.47	138.83	1.05
1:1.125	162	0.46	135.88	1.03
1:1.5	163	0.45	132.93	1.01

[a] Values are determined by converting the data in column three using the mass of the monomer unit of PSBA, 295.39g mol^{-1}.

[b] Values are determined by dividing the data in column four by 132J mol^{-1} K^{-1}.

dynamic is shown here. The high crosslinking density in the polyzwitterion without salt confines the polymer which drives the glass transition to higher temperatures; when the crosslinks are removed by salt addition, T_g is reduced, and the liquid state heat capacity is increased.

The glass transition temperatures and heat capacity increments at T_g for PSBA-LiCl complexes are reported in Table 2. The lowest glass transition temperature reported is 158±1°C for the complex with molar salt ratio SBA:LiCl 1:0.77. However, further salt addition resulted in a slight increase in the glass transition temperature to 163±1°C for all PSBA-LiCl complexes at or above 1:1 SBA:LiCl ratio. Conversely the highest heat capacity increment at T_g was seen in the 1:1 complex while further salt addition resulted in a small decrease, though within the error limits of the measurement. LiCl acts as a plasticizing agent in our PZIs, up to high molar salt ratios (~1:1.8). LiCl has low molecular size and low polarizability, so the dissociation of the salt ions on the zwitterionic moiety is highly likely. The free ions act as a plasticization agent for the polyzwitterion chains, consistent with the observations of Galin, et al. [19]. With Li^+ as the cation, Galin, et al. studied the effects of bulkiness and polarizability for a variety of anions, including BF_4^-, SCN^-, ClO_4^-, and $B(C_6H_5)_4^-$. Unlike LiCl, these more bulky and highly polarizable salts act as anti-plasticizers due to complex interactions with the polymer chains.

Using the Wunderlich empirical bead approximation of a polymer, each freely rotatable bond of the monomer unit contributes approximately 11J mol^{-1} K^{-1} to the heat capacity increment at T_g (exclusive of C—O and double bonds) [48]. For the PSBA monomer with 12 freely rotatable bonds (shown in the inset of Fig. 10) the heat capacity increment, Δc_p^{bead}, is 132J mol^{-1} K^{-1}. [48,49]. The measured heat capacity increment in J g^{-1} K^{-1} is converted to J mol^{-1} K^{-1} using the molecular weight of the PSBA monomer, 295.39g mol^{-1}. Normalizing the measured heat capacity increment to the bead model's predicted heat capacity increment, Fig. 10 shows the fully mobile (unconfined) state, marked by the black cross-hair, is reached at and above ZI:LiCl 1:1 where it is believed that all dipolar crosslinks have been broken through ion association. Error bars here are based on the reported 2% uncertainty in heat capacity measurement in the DSC. As salt is reduced below the 1:1 molar salt content, the ratio of $\Delta c_p(T_g)/\Delta c_p^{bead}$ decreases, which can be interpreted as a reduction in the number of freely rotatable bonds contributing to the glass transition process.

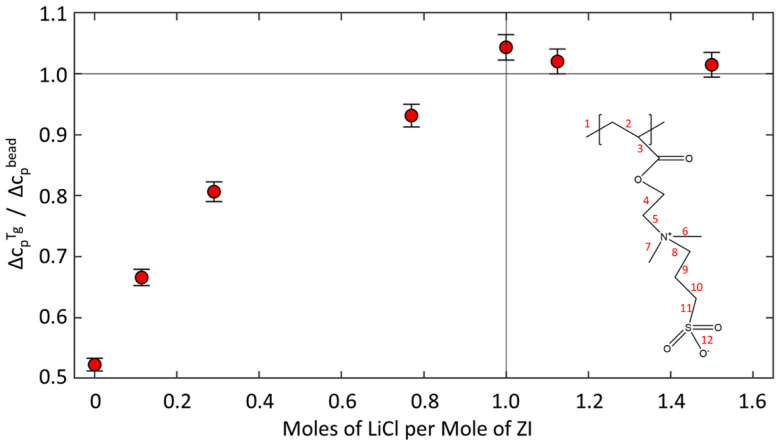

Fig. 10. Ratio of the heat capacity increment at T_g to the heat capacity increment predicted by Wunderlich's empirical bead model, as a function of molar salt content for PSBA-LiCl complexes. Black crosshair represents the theoretical unconfined state. The inset shows PSBA chemical structure indicating the 12 freely rotatable bonds, each of which contributes ~11J mol^{-1} K^{-1} to the heat capacity increment at T_g [48,49].

4. Conclusions

Successful disruption of the dipolar crosslinking in three PZIs was achieved by the association of LiCl salt ions onto the side groups even above the 1:1 ZI:LiCl content, as confirmed through FTIR. This disruption in crosslinking was shown to decrease the average interatomic d-spacing seen in WAXS. The side group thermal stability is directly related to the crosslinking as shown by the decrease in onset of degradation in thermogravimetry as the salt content is increased, and the stabilizing crosslinks are lost. The glass transition dynamics were successfully isolated from the water plasticization through both the Ratchet Method used in DSC and the modified Ratchet Method in TMDSC.

For the polyzwitterions studied here, electrostatic dipolar crosslinking of the side-groups results in reduced molecular mobility. We see several similarities of behavior between PZIs and semicrystalline polymers. In the case of semicrystalline polymers, crystals confine the amorphous phase causing reduced molecular mobility resulting in higher glass transition temperatures and smaller heat capacity increments in the semicrystalline state than in the completely amorphous state. Here, the polyzwitterion PZI without added salt has reduced molecular mobility, as shown by the higher glass transition temperatures and reduced liquid-state heat capacity, yielding a smaller heat capacity increment, compared to PZI with added LiCl salt.

One notable difference is seen between the crosslinked PZIs and semicrystalline polymers, *viz.*, the breadth of the glass transition. Amorphous crystallizable polymers have generally narrower breadths of the glass transition than their semicrystalline counterparts. We did not observe that behavior in the PZIs with added salt. Apparently, addition of LiCl salt to PZIs results in a similar spread of relaxation times for molecules undergoing the glass transition.

Comparing heat capacity data with Wunderlich's empirical bead model estimate [37], the fully mobile, unconfined state of the PZI was achieved at high molar salt content, at or above the ZI:LiCl 1:1 composition. This provides a strong fundamental understanding of both zwitterionic interactions through chemical variations as well as the effects of added small molecule LiCl salt on the crosslinking, structural, and thermal properties.

CRediT authorship contribution statement

John Thomas: Investigation, Software, Visualization, Writing – original draft, Writing – review & editing. **Sammie Chum:** Investigation. **William Deucher:** Investigation. **Abhishek Mondal:** Resources. **Ayse Asatekin:** Resources, Writing – review & editing, Conceptualization, Supervision, Funding acquisition. **Peggy Cebe:** Visualization, Conceptualization, Supervision, Funding acquisition, Writing – review & editing.

Declaration of Competing Interest

The authors declare that they have no known competing financial interests or personal relationships that could have appeared to influence the work reported in this paper.

Data availability

Data will be made available on request.

Acknowledgments

Support for this research was provided by the National Science Foundation, Polymers Program of the Division of Materials Research, under grant DMR-2003629.

Supplementary materials

Supplementary material associated with this article can be found, in the online version, at doi:10.1016/j.tca.2023.179617.

References

[1] R. Kumar, G.H. Fredrickson, Theory of polyzwitterion conformations, J. Chem. Phys. 131 (10) (2009), https://doi.org/10.1063/1.3216107. ISSN 0021-9606 10.1063/1. 3216107. URL.

[2] A. Laschewsky, Structures and synthesis of zwitterionic polymers, Polymers 6 (5) (2014) 1544–1601. BaselISSN 2073-4360. URL, https://www.mdpi.com/2073-4360/6/5/1544.

[3] M. Ilčíková, J. Tkač, P. Kasak, Switchable materials containing polyzwitterion moieties, Polymers 7 (11) (2015) 2344–2370. BaselISSN 2073-4360. URL, https://www.mdpi.com/2073-4360/7/11/1518.

[4] R. Lalani, L. Liu, Electrospun zwitterionic poly(sulfobetaine methacrylate) for nonadherent, superabsorbent, and antimicrobial wound dressing applications, Biomacromolecules 13 (6) (2012) 1853–1863, https://doi.org/10.1021/bm300345e. URL, https://www.scopus.com/inward/record.uri?eid=2-s2.0-84862136918&doi=10.1021%2fbm300345e&partnerID=40&md5=1057acaf3dc172ed01f0818fd8e807b9.

[5] S. Paschke, K. Lienkamp, Polyzwitterions: from surface properties and bioactivity profiles to biomedical applications, ACS Appl. Polym. Mater. 2 (2) (2020) 129–151, https://doi.org/10.1021/acsapm.9b00897, 10.1021/acsapm.9b00897. URL.

[6] J.T. Sun, Z.Q. Yu, C.Y. Hong, C.Y. Pan, Biocompatible zwitterionic sulfobetaine copolymer-coated mesoporous silica nanoparticles for temperature-responsive drug release, Macromol. Rapid Commun. 33 (9) (2012) 811–818, https://doi.org/10.1002/marc.201100876. ISSN 1022-1336URL, https://onlinelibrary.wiley.com/doi/abs/10.1002/marc.201100876.

[7] W. Yang, H. Xue, L.R. Carr, J. Wang, S. Jiang, Zwitterionic poly(carboxybetaine) hydrogels for glucose biosensors in complex media, Biosens. Bioelectron. 26 (5) (2011) 2454–2459, https://doi.org/10.1016/j.bios.2010.10.031. ISSN 0956-5663URL, https://www.sciencedirect.com/science/article/pii/S0956566310007165.

[8] N. Govinna, P. Kaner, D. Ceasar, A. Dhungana, C. Moers, K. Son, A. Asatekin, P. Cebe, Electrospun fiber membranes from blends of poly(vinylidene fluoride) with fouling-resistant zwitterionic copolymers, Polym. Int. 68 (2) (2019) 231–239, https://doi.org/10.1002/pi.5578. ISSN 0959-8103URL, https://onlinelibrary.wiley.com/doi/abs/10.1002/pi.5578.

[9] DoH Kim, and P. Kaner, E. Rubakh, A. Asatekin, Zwitterion-containing polymer additives for fouling resistant ultrafiltration membranes, J. Memb. Sci. 533 (2017) 141–159, https://doi.org/10.1016/j.memsci.2017.03.034. ISSN 0376-7388URL, https://www.sciencedirect.com/science/article/pii/S0376738817304635.

[10] S. Ray, R.P. Cooney, Thermal Degradation of Polymer and Polymer Composites. Handbook of Environmental Degradation of Materials, third ed, Elsevier, Oxford, 2018, pp. 185–206, https://doi.org/10.1016/B978-0-323-52472-8.00009-5.URL https://www.sciencedirect.com/science/article/pii/B9780323524728000095.

[11] F.M. Uhl, G.F. Levchik, S.V. Levchik, C. Dick, J.J. Liggat, C.E. Snape, C.A. Wilkie, The thermal stability of cross-linked polymers: methyl methacrylate with divinylbenzene and styrene with dimethacrylates, Polym. Degrad. Stab. 71 (2) (2001) 317–325, https://doi.org/10.1016/S0141-3910(00)00181-6. ISSN 0141-3910URL, https://www.sciencedirect.com/science/article/pii/S0141391000001816.

[12] J. Cardoso, O. Soria-Arteche, G. Vażquez, O. Solorza, I. Gonzalez, Synthesis and characterization of Zwitterionic polymers with a flexible lateral chain, J. Phys. Chem. C 114 (33) (2010) 14261–14268. ISSN 1932-7447.

[13] M.E. Taylor, D. Clarkson, S.G. Greenbaum, M.J. Panzer, Examining the impact of polyzwitterion chemistry on lithium ion transport in ionogel electrolytes, ACS Appl. Polym. Mater. 3 (5) (2021) 2635–2645, https://doi.org/10.1021/acsapm.1c00229, 10.1021/acsapm.1c00229. URL.

[14] S. Wang, D. Zhang, X. He, J. Yuan, W. Que, Y. Yang, I. Protsak, X. Huang, C. Zhang, T. Lu, P. Pal, S. Liu, S.Y. Zheng, J. Yang, Polyzwitterionic doublenetwork ionogel electrolytes for supercapacitors with cryogenic-effective stability, Chem. Eng. J. 438 (2022), 135607, https://doi.org/10.1016/j.cej.2022.135607. ISSN 1385-8947URL, https://www.sciencedirect.com/science/article/pii/S1385894722011093.

[15] L. Zhang, H. Gao, L. Guan, Y. Li, Q. Wang, Polyzwitterionn-SiO2 double-network polymer electrolyte with high strength and high ionic conductivity, Polymers 15 (2) (2023) 466. BaselISSN 2073-4360. URL, https://www.mdpi.com/2073-4360/15/2/466.

[16] C. Vachon, M. Vasco, M. Perrier, J. Prud'homme, Microphase separation in amorphous polyethers complexed with lithium perchlorate, sodium perchlorate and sodium iodide, Macromolecules 26 (15) (1993) 4023–4031, https://doi.org/10.1021/ma00067a045, doi: 10.1021/ma00067a045 URL.

[17] C. Vachon, C. Labreche, A. Vallee, S. Besner, M. Dumont, J. Prud'homme, Microphase separation and conductivity behavior of poly(propulene oxide)-lithium salt electrolytes, Macromolecules 28 (16) (1995) 5585–5594, https://doi.org/10.1021/ma00120a025, 10.1021/ma00120a025 URL.

[18] F. Fan, Y. Wang, A.P. Sokolov, Ionic Transport, microphase separation, and polymer relaxation in poly(propylene glycol) and lithium perchlorate mixtures, Macromolecules 46 (23) (2013) 9380–9389, https://doi.org/10.1021/ma401238k, doi: 10.1021/ma401238k URL.

[19] M. Galin, E. Marchal, A. Mathis, J.C. Galin, Poly(ammonioalkanesulfonate) blends with polar organic species and alkali metal salts: structure, glass transition and ionic conductivity, Polym. Adv. Technol. 8 (2023) 75–86, doi.org/10.1002/(SICI)1099-1581(199702)8:2<75::AID−PAT622>3.0.CO;2-W. URL 10.1002/(SICI)1099-1581(199702)8:2<75::AID−PAT622>3.0.CO;2-W.

[20] A. Clark, Y. Biswas, M.E. Taylor, A. Asatekin, M.J. Panzer, C. Schick, P. Cebe, Glass-forming ability of polyzwitterions, Macromolecules 54 (21) (2021) 10126–10134, https://doi.org/10.1021/acs.macromol.1c01393. ISSN 0024-9297 10. 1021/acs.macromol.1c01393. URL.

[21] G. Ten Brinke, F.E. Karasz, T.S. Ellis, Depression of glass transition temperatures of polymer networks by diluents, Macromolecules 16 (2) (1983) 244–249, https://doi.org/10.1021/ma00236a017, doi.org/10.1021/ma00236a01. URL.

[22] S.D. Cheng, M.Y. Cao, B. Wunderlich, Glass transition and melting behavior of poly (oxy- 1,4-phenyleneoxy- 1,4-phenylenecarbonyl- 1,4-phenylene) (PEEK), Macromolecules 19 (1986) 1868–1876, https://doi.org/10.1021/ma00161a015, doi.org/10.1021/ma00161a015. URL.

[23] R. Androsch, B. Wunderlich, The link between rigid amorphous fraction and crystal perfection in cold-crystallized poly(ethylene terephthalate), Polymer 46 (2005) 12556–12566, https://doi.org/10.1016/j.polymer.2005.10.099. Guildfdoi.org/10.1016/j.polymer.2005.10.099. URL.

[24] A. Sargsyan, A. Tonoyan, S. Davtyan, C. Schick, The amount of immobilized polymer in PMMA SiO2 nanocomposites determined from calorimetric data, Eur. Polym. J. 43 (2007) 3113–3127, https://doi.org/10.1016/j.eurpolymj.2007.05.011, doi.org/10.1016/j.eurpolymj.2007.05.011. URL.

[25] P. Cebe, B.P. Partlow, D.L. Kaplan, A. Wurm, E. Zhuravlev, C. Schick, Silk I and silk II studied by fast scanning calorimetry, Acta Biomater. 55 (2017) 323–332, https://doi.org/10.1016/j.actbio.2017.04.001, doi.org/10.1016/j.actbio.2017.04.001. URL.

[26] X. Hu, D. Kaplan, P. Cebe, Determining beta sheet crystallinity in fibrous proteins by thermal analysis and infrared spectroscopy, Macromolecules 39 (2006) 6161–6170, https://doi.org/10.1021/ma0610109, doi.org/10.1021/ma0610109. URL.

[27] M.J. Schroeder, C.M. Roland, Segmental relaxation in end-linked poly (dimethylsiloxane) networks, Macromolecules 35 (7) (2002) 2676–2681, 10.1021/ma011678h URL 10.1021/ma011678h.

[28] J.K.W. Glatz-Reichenbach, L. Sorriero, J.J. Fitzgerald, Influence of crosslinking on the molecular relaxation of an amorphous copolymer near its glass-transition temperature, Macromolecules 27 (6) (1994) 1338–1343, https://doi.org/10.1021/ma00084a010, doi: 10.1021/ma00084a010 URL.

[29] C.M. Roland, Constraints on local segmental motion in poly(vinylethylene) networks, Macromolecules 27 (15) (1994) 4242–4247, https://doi.org/10.1021/ma00093a027, doi: 10.1021/ma00093027 URL.

[30] V.Y. Kramarenko, T.A. Ezquerra, I. Šics, F.J. Baltá-Calleja, V.P. Privalko, Influence of cross-linking on the segmental dynamics in model polymer networks, J. Chem. Phys. 113 (2023) 447–452, https://doi.org/10.1063/1.481809, 10.1063/1.481809 URL.

[31] N.M. Alves, J.L. Gómez Ribelles, J.A. Gómez Tejedor, J.F. Mano, Viscoelastic behavior of poly(methyl methacrylate) networks with different cross-linking degrees, Macromolecules 37 (10) (2004) 3735–3744, https://doi.org/10.1021/ma035626z, doi: 10.1021/ma035626z URL.

[32] S. Kalakkunnath, D.S. Kalika, H. Lin, B.D. Freeman, Segmental relaxation characteristics of cross-linked poly(ethylene oxide) copolymer networks, Macromolecules 38 (23) (2005) 9679–9687, https://doi.org/10.1021/ma051741t, doi: 10.1021/ma051741t URL.

[33] A. Shundo, M. Aoki, S. Yamamoto, Cross-linking effect of segmental dynamics of well-defined epoxy resins, Macromolecules 54 (13) (2021) 5950–5956, https://doi.org/10.1021/acs.macromol.1c00513, doi: 10.1021/acs.macromol.1c00513 URL.

[34] E.A. DiMarzio, On the second-order transition of a rubber, J. Res. Nation Bur. Stand. A. Phys. Chem. 68A (6) (1964) 611–617, https://doi.org/10.6028/jres.068A.059, doi: 10.6028/jres.068A.059 URL.

[35] A. Clark, M. Rosenbaum, Y. Biswas, A. Asatekin, P. Cebe, Heat Capacity and index of refraction of polyzwitterions, Polymer 256 (2022), 125176, https://doi.org/10.1016/j.polymer.2022.125176. Guildfdoi: 10.1016/j.polymer.2022.125176 URL.

[36] C.T. Moynihan, A.J. Easteal, M.A.D. Bolt, J. Tucker, Dependence of the fictive temperature of glass on cooling rate, J. Am. Ceram. Soc. 59 (1–2) (1976) 12–16, https://doi.org/10.1111/j.1151-2916.1976.tb09376. ISSN 0002-7820URL, https://ceramics.onlinelibrary.wiley.com/doi/abs/10.1111/j.1151-2916.1976.tb09376.x.

[37] D.A. Ditmars, S. Ishihara, S.S. Chang, G. Bernstein, E.D. West, Enthalpy and heat-capacity standard reference material: synthetic sapphire (Al(2)O(3)) from 10 to 2250 k, J. Res. Natl. Bur. Stand. 87 (2) (1982) 159–163, https://doi.org/10.6028/jres.087.012 (1977)ISSN 0160-1741 (Print) 0160-1741.

[38] X. Hu, D. Kaplan, P. Cebe, Effect of water on the thermal properties of silk fibroin, Thermochim. Acta 461 (1) (2007) 137–144, https://doi.org/10.1016/j.tca.2006.12.011. ISSN 0040-6031URL, https://www.sciencedirect.com/science/article/pii/S0040603106006289.

[39] The Engineering ToolBox, Water - Specific Heat vs. Temperature, https://www.engineeringtoolbox.com/specific-heat-capacity-water-d_660.html. 2021, (Accessed September 2021).

[40] MilliporeSigma,IR Spectrum Table & Chart, https://www.sigmaaldrich.com/US/en/technical-documents/technical-article/analytical-chemistry/photometry-and-reflectometry/ir-spectrum-table. 2021, (Accessed September 2021).

[41] Y.S. Kim, L.M. Dong, M.A. Hickner, T.E. Glass, V. Webb, J.E. McGrath, State of water in disulfonated poly(arylene ether sulfone) copolymers and a perfluorosulfonic acid copolymer (nafion) and its effect on physical and electrochemical properties, Macromolecules 36 (2003) 6281–6285, https://doi.org/10.1021/ma0301451, doi.org/10.1021/ma0301451. URL.

[42] P. Peyser, W.D. Bascom, The anomalous lowering of the glass transition of an epoxy resin by plasticization with water, J. Mater. Sci. 16 (1) (1981) 75–83, https://doi.org/10.1007/BF00552061. ISSN 1573-4803 10.1007/BF00552061URL.

[43] W. Huang, S. Krishnaji, X. Hu, D. Kaplan, P. Cebe, Heat capacity of spider silk-like block copolymers, Macromolecules 44 (13) (2011) 5299–5309, https://doi.org/10.1021/ma200563t. ISSN 0024-9297 10.1021/ma200563tURL.

[44] W. Huang, S. Krishnaji, O.R. Tokareva, D. Kaplan, P. Cebe, Influence of water on protein transitions: thermal analysis, Macromolecules 47 (22) (2014) 8098–8106, https://doi.org/10.1021/ma5016215. ISSN 0024-9297 10.1021/ma5016215URL.

[45] H. Xu, P. Cebe, Heat capacity study of isotactic polystyrene: dual reversible crystal melting and relaxation of rigid amorphous fraction, Macromolecules 37 (8) (2004) 2797–2806, https://doi.org/10.1021/ma035961n. ISSN 0024-9297 10.1021/ma035961n. URL.

[46] M.W. Chase Jr, NIST-JANAF themochemical tables, fourth edition, J. Phys. Chem. Ref. Data Monogr. 9 (1998) 758.

[47] O. Nordness, J.F. Brennecke, Ion dissociation in ionic liquids and ionic liquid solutions, Chem. Rev. 120 (23) (2020) 12873–12902, https://doi.org/10.1021/acs.chemrev.0c00373. ISSN 00092665URL 10.1021/acs. chemrev.0c00373.

[48] B. Wunderlich, J. Grebowicz, Thermotropic mesophases and mesophase transitions of linear, flexible macromolecules, Adv. Polym. Sci. (1984) 1–59, https://doi.org/10.1007/3-540-12994-4_1, 60-1.

[49] B. Wunderlich, L.D. Jones, Heat capacities of solid polymers, J. Macromol. Sci. Phys. B 3 (1) (1969) 67–79, https://doi.org/10.1080/00222346908217089.